

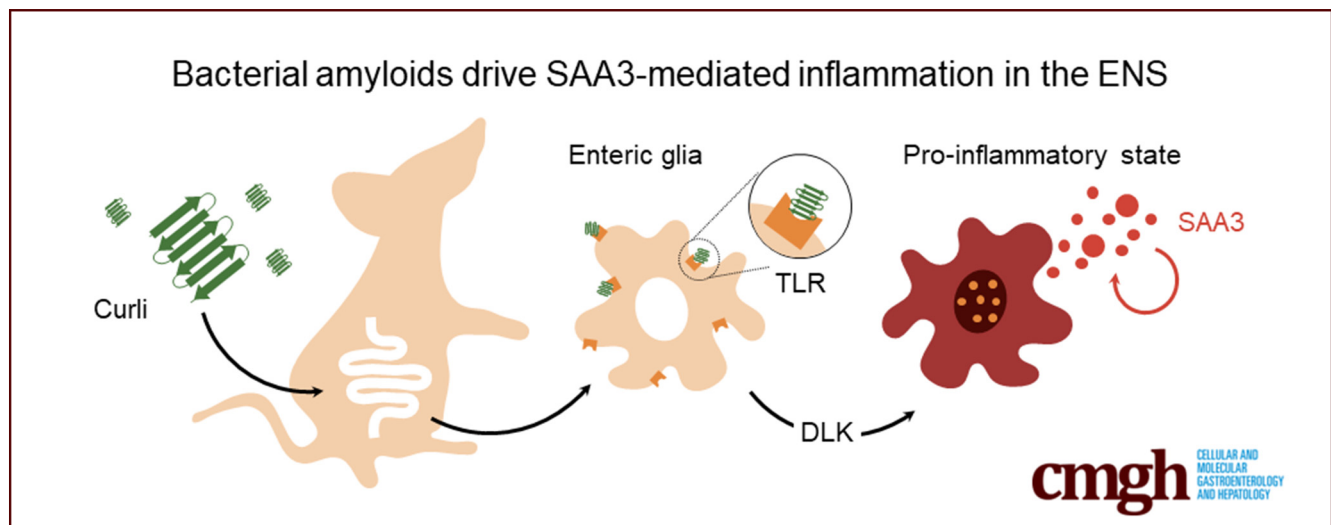
## ORIGINAL RESEARCH

## Serum Amyloid A3 Fuels a Feed-Forward Inflammatory Response to the Bacterial Amyloid Curli in the Enteric Nervous System



Peter Verstraelen,<sup>1</sup> Samuel Van Remoortel,<sup>1</sup> Nouchin De Loose,<sup>1</sup> Rosanne Verboven,<sup>1</sup> Gerardo Garcia-Diaz Barriga,<sup>1</sup> Anne Christmann,<sup>2</sup> Manuela Gries,<sup>2</sup> Shingo Bessho,<sup>3</sup> Jing Li,<sup>4</sup> Carmen Guerra,<sup>4,5</sup> Çağla Tükel,<sup>3</sup> Sales Ibiza Martinez,<sup>1</sup> Karl-Herbert Schäfer,<sup>2</sup> Jean-Pierre Timmermans,<sup>1,6,7,§</sup> and Winnok H. De Vos<sup>1,6,7,§</sup>

<sup>1</sup>Laboratory of Cell Biology and Histology, University of Antwerp, Wilrijk, Belgium; <sup>2</sup>Working Group Enteric Nervous System, University of Applied Sciences Kaiserslautern, Zweibrücken, Germany; <sup>3</sup>Center for Microbiology and Immunology, Lewis Katz School of Medicine, Temple University, Philadelphia, Pennsylvania; <sup>4</sup>Experimental Oncology Group, Centro Nacional de Investigaciones Oncológicas, Madrid, Spain; <sup>5</sup>Centro de Investigación Biomédica en Red de Cáncer, Instituto de Salud Carlos III, Madrid, Spain; <sup>6</sup>Antwerp Centre for Advanced Microscopy, University of Antwerp, Antwerp, Belgium; and <sup>7</sup>μNeuro Research Centre of Excellence, University of Antwerp, Antwerp, Belgium



## SUMMARY

Epidemiologic associations and preclinical studies suggest that amyloid pathology observed in the brain may be preceded by gastrointestinal amyloidosis. We identify a pathogenic program that becomes activated in the enteric nervous system after exposure to bacterial amyloids, and show that serum amyloid A3 is an important self-amplifying mediator of this proinflammatory response.

**BACKGROUND & AIMS:** Mounting evidence suggests the gastrointestinal microbiome is a determinant of peripheral immunity and central neurodegeneration, but the local disease mechanisms remain unknown. Given its potential relevance for early diagnosis and therapeutic intervention, we set out to map the pathogenic changes induced by bacterial amyloids in the gastrointestinal tract and its enteric nervous system.

**METHODS:** To examine the early response, we challenged primary murine myenteric networks with curli, the

prototypical bacterial amyloid, and performed shotgun RNA sequencing and multiplex enzyme-linked immunosorbent assay. Using enteric neurosphere-derived glial and neuronal cell cultures, as well as *in vivo* curli injections into the colon wall, we further scrutinized curli-induced pathogenic pathways.

**RESULTS:** Curli induced a proinflammatory response, with strong up-regulation of *Saa3* and the secretion of several cytokines. This proinflammatory state was induced primarily in enteric glia, was accompanied by increased levels of DNA damage and replication, and triggered the influx of immune cells *in vivo*. The addition of recombinant Serum Amyloid A3 (SAA3) was sufficient to recapitulate this specific proinflammatory phenotype while *Saa3* knock-out attenuated curli-induced DNA damage and replication. Similar to curli, recombinant SAA3 caused a strong up-regulation of *Saa3* transcripts, illustrating its self-amplifying potential. Since colonization of curli-producing *Salmonella* and dextran sulfate sodium-induced colitis triggered a significant increase in *Saa3* transcripts as well, we assume SAA3 plays a central role in enteric dysfunction. Inhibition of dual leucine zipper kinase, an upstream regulator of the c-Jun N-terminal kinase pathway

responsible for SAA3 production, attenuated curli- and recombinant SAA3-induced *Saa3* up-regulation, DNA damage, and replication in enteric glia.

**CONCLUSIONS:** Our results position SAA3 as an important mediator of gastrointestinal vulnerability to bacterial-derived amyloids and demonstrate the potential of dual leucine zipper kinase inhibition to dampen enteric pathology. (*Cell Mol Gastroenterol Hepatol* 2024;18:89–104; <https://doi.org/10.1016/j.jcmgh.2024.03.013>)

**Keywords:** Microbiome–Gut–Brain Axis; Curli; Enteric Nervous System; Serum Amyloid A3; Dual Leucine Zipper Kinase.

Recent epidemiologic and preclinical studies have shown that the risk of developing Parkinson's disease or Alzheimer's disease (AD) can be exacerbated by inflammation in the gastrointestinal (GI) tract. Patients with inflammatory bowel disease (relapsing-remitting GI inflammation) have a higher risk of developing dementia than healthy individuals.<sup>1,2</sup> A potential driver of this peripheral inflammation is the enteric microbiome.<sup>3</sup> Indeed, both Parkinson's disease and AD patients display disease-permissive enteric dysbiosis with overrepresentation of immunogenic pathogens and reduced microbial production of anti-inflammatory and neuroprotective factors.<sup>4,5</sup>

Bacteria may contribute to peripheral inflammation and central neurodegenerative pathology through secretion of curli. This functional bacterial amyloid is synthesized and secreted for cell attachment and biofilm formation.<sup>6</sup> It constitutes a pathogen-associated molecular pattern that is recognized by the host's innate immune system through Toll-like receptor (TLR) binding and is therefore an important determinant of gastrointestinal immunity.<sup>7,8</sup> Curli signals through TLR1 and TLR2, and the fibrils additionally contain nucleic acids that activate endosomal TLR9, as shown in human (THP-1) and murine immortalized macrophages.<sup>9,10</sup> In *Caenorhabditis elegans*, curli was the top hit in a genome-wide screen aimed at identifying bacterial genes that promote host neurodegeneration.<sup>11</sup> Curli, secreted by bacteria that were fed to the worms, promoted neuronal  $\alpha$ -synuclein aggregation and enhanced mitochondrial dysfunction and neuronal cell death.<sup>11</sup> Similarly, GI colonization with curli-producing *Escherichia coli* promoted  $\alpha$ -synuclein deposits in the gut and brain of aged rats, along with central astrogliosis and microgliosis.<sup>12</sup> A similar colonization approach enhanced motor deterioration in Thy1- $\alpha$ Syn mice, plausibly as a result of its cross-seeding and co-aggregation potential.<sup>13</sup> These studies showed that microbial amyloid can trigger a systemic immune response and accelerate central neurodegeneration.

To eventually develop novel diagnostic or treatment options in an early disease state, it is key to understand the local response to bacterial amyloids in the GI tract and its enteric nervous system (ENS), defined as the network of neurons and glia located in the GI wall. Because the nature of the pathogenic response is unknown, or which cell types and disease mediators are involved, we have challenged

myenteric networks with curli, and studied the downstream pathogenic events in different *in vitro* and *in vivo* models.

## Results

### *The Bacterial Amyloid Curli Triggers a Proinflammatory Response in Primary Myenteric Networks*

To determine whether bacterial amyloids affect the ENS, we isolated primary myenteric networks from adult C57BL/6N mice and challenged them with curli (vs culture medium). Twenty-four hours later, we analyzed the transcriptome via bulk RNA-sequencing (RNA-seq) (Figure 1A). As internal validation, we inspected characteristic cell type marker genes, which revealed that the primary networks consisted mainly of neurons (*Uchl1*, *Tubb3*, *Nefl*), enteric glia (*Sox10*, *S100b*, *Gfap*), and, to a lesser extent, smooth muscle cells (*Cald1*, *Acta2*) (Figure 1B). Interstitial cells of Cajal (*Kit*, *Ano1*) and immune cells were absent (*Tpsab1*, *Ptprc*, *Itgax*, *Itgam*, *H2-Ab1*, *Fcgr1*, *Cx3cr1*, *Cma1*, *Cd8a*, *Cd4*, *Cd3d*, *Cd169*, *Arg1*, *Aif1*, *Adgre1* below detection limit). When homing in on genes with a log<sub>2</sub> fold change >5, we noticed that a distinct set of curli-induced genes pertained to innate immune activation (Figure 1C). Among those, *Saa3*, a well-known acute phase reactant with amyloidogenic properties, was the top hit. To verify whether this expression profile was accompanied by a canonical inflammatory response, we quantified secreted cytokines in the culture medium by multiplex enzyme-linked immunosorbent assay (ELISA) (Figure 1D). Curli induced the release of the pyrogen interleukin 1 $\beta$ , and the chemokine (C-X-C motif) ligand 1 (CXCL1), CXCL2, chemokine (C-C motif) ligand 2 (CCL2), CCL3, and CCL5. This showed that myenteric networks launch an inflammatory response when confronted with the bacterial amyloid curli, even in a model that is devoid of the typical immune cells.

### *Enteric Glia Are an Important Source of the Curli-Induced Immune Response*

To determine the cellular origin of the proinflammatory cytokines, we differentiated primary enteric neurospheres

<sup>§</sup>Authors share co-senior authorship.

**Abbreviations used in this paper:** AD, Alzheimer's disease; cDNA, complementary DNA; CCL, chemokine (C-C motif) ligand; CXCL, chemokine (C-X-C motif) ligand; DLK, dual leucine zipper kinase; DMEM, Dulbecco's modified Eagle medium; DSS, dextran sulfate sodium; E14, embryonic day 14; EdU, 5-ethynyl-2'-deoxyuridine; ELISA, enzyme-linked immunosorbent assay; ENS, enteric nervous system; FACS, fluorescence-activated cell sorter; GI, gastrointestinal; JNK, c-Jun N-terminal kinase; LPS, lipopolysaccharide; mRNA, messenger RNA; NA, numerical aperture; PBS, phosphate-buffered saline; Pen/Strep, Penicillin and streptomycin; PFA, paraformaldehyde; qPCR, quantitative polymerase chain reaction; rSAA3, recombinant serum amyloid A3; SAA3, serum amyloid A3; SOX10, SRY-box transcription factor 10; TBS-T, Tris-buffered saline with 0.1% Tween; TLR, Toll-like receptor;  $\gamma$ H2AX, gamma-histone variant H2AX.



Most current article

© 2024 The Authors. Published by Elsevier Inc. on behalf of the AGA Institute. This is an open access article under the CC BY-NC-ND license (<http://creativecommons.org/licenses/by-nc-nd/4.0/>).

2352-345X

<https://doi.org/10.1016/j.jcmgh.2024.03.013>

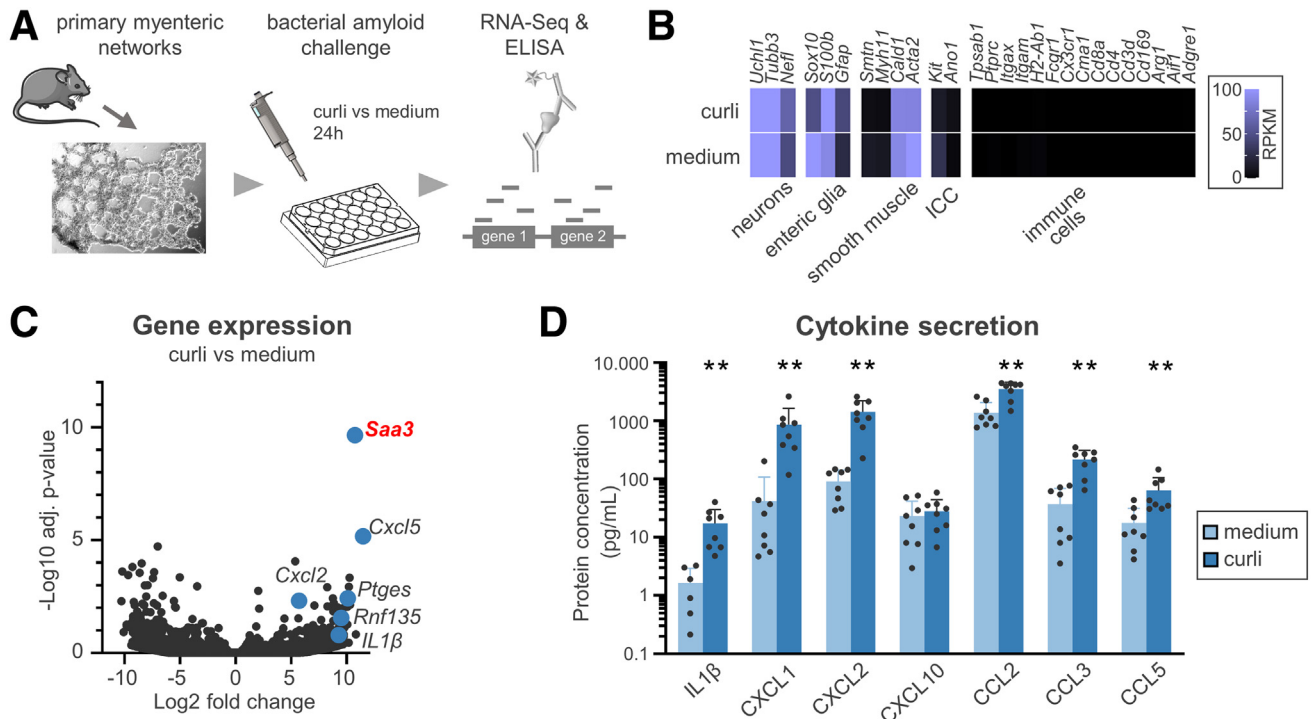


**Figure 1. The bacterial amyloid curli triggers a proinflammatory response in primary myenteric networks.** (A) Experimental workflow. Primary myenteric networks were isolated from adult mouse colon and challenged with bacterial amyloid for 24 hours. Medium was collected for multiplex ELISA and cell lysates processed for bulk RNA-seq. (B) Expression levels of canonical cell type markers, expressed in reads per kilo base per million mapped reads (RPKM). (C) Volcano plot showing that many curli up-regulated transcripts pertain to a proinflammatory response. (D) Concentrations of proinflammatory cytokines and chemokines released into the culture medium. Means + SD;  $n = 8$  animals. Two-way analysis of variance on log-transformed data: treatment  $P < .005$ , analyte  $P < .005$ , analyte\*treatment  $P < .005$ ; \*\* $P < .005$  in  $t$  test with Holm-Sidak correction. adj., adjusted; ICC, interstitial cells of Cajal; IL, interleukin.

to cultures enriched for enteric glia or enteric neurons (Figure 2A). We opted for this model because myenteric networks are very fragile and ganglia are packed too densely to untangle the cell types. Although neurosphere-derived glial cultures contained a mixture of enteric glia (glial fibrillary acidic protein<sup>+</sup>) and smooth muscle cells ( $\alpha$ -smooth muscle actin<sup>+</sup> and SRY-box transcription factor 10 [SOX10]<sup>+</sup>), the neuronal cultures were enriched in enteric neurons ( $\beta$ III-tubulin<sup>+</sup>), but also contained a lower amount of glia and smooth muscle cells (Figure 2B). Therefore, we further refer to these cultures as *enteric glia-enriched* and *neuron-enriched* cultures, respectively. Consistent with our observations in primary myenteric networks, quantitative polymerase chain reaction (qPCR) analysis showed a marked up-regulation of *Saa3*, which was more pronounced in enteric glia-enriched than in neuron-enriched cultures (Figure 2C). Similarly, glia-enriched cultures secreted higher cytokine levels in the culture medium than neurons in response to curli exposure (Figure 2D). In fact, in glia-enriched cultures, curli evoked a response that was similar in amplitude and cytokine profile to lipopolysaccharide (LPS), a well-known TLR4 agonist (Figure 2C and D). In enteric neuron-enriched cultures, no response was observed after LPS stimulation whereas curli induced limited *Saa3* up-regulation (Figure 2C) and cytokine release (Figure 2D), indicating that LPS and curli activate different

receptors. These experiments showed that curli induces a similar immune response in the neurosphere-derived cellular model, and that enteric glia are a source of the secreted factors.

### Curli Induces DNA Damage and Replication In Vitro

In parallel with the inflammatory response, we found that curli elicited a transcriptional signature of cell-cycle dysregulation in primary myenteric networks (Figure 3A; enriched term clusters: cell division, [negative] regulation of cell-cycle phase transition). An associated transcriptional hub inferred curli in the DNA damage response (Figure 3A; intrinsic apoptotic signaling pathway in response to DNA damage, DNA repair pathways full network, response to radiation). To further scrutinize curli's potential for inducing DNA damage, we quantified nuclear gamma-histone variant H2AX ( $\gamma$ H2AX) spots in glia-enriched cultures, a well-established marker for double-stranded DNA breaks (Figure 3B and C). Curli treatment for 24 hours increased the proportion of  $\gamma$ H2AX-positive nuclei (defined as nuclei with  $\geq 5$   $\gamma$ H2AX spots) in all cells, and in SOX10<sup>+</sup> (ie, glial) cells specifically. To confirm the observed cell-cycle dysregulation in these cultures we also performed 5-ethynyl-2'-deoxyuridine (EdU) replication labeling during the last 4 hours of amyloid exposure (Figure 3B and D). Surprisingly,

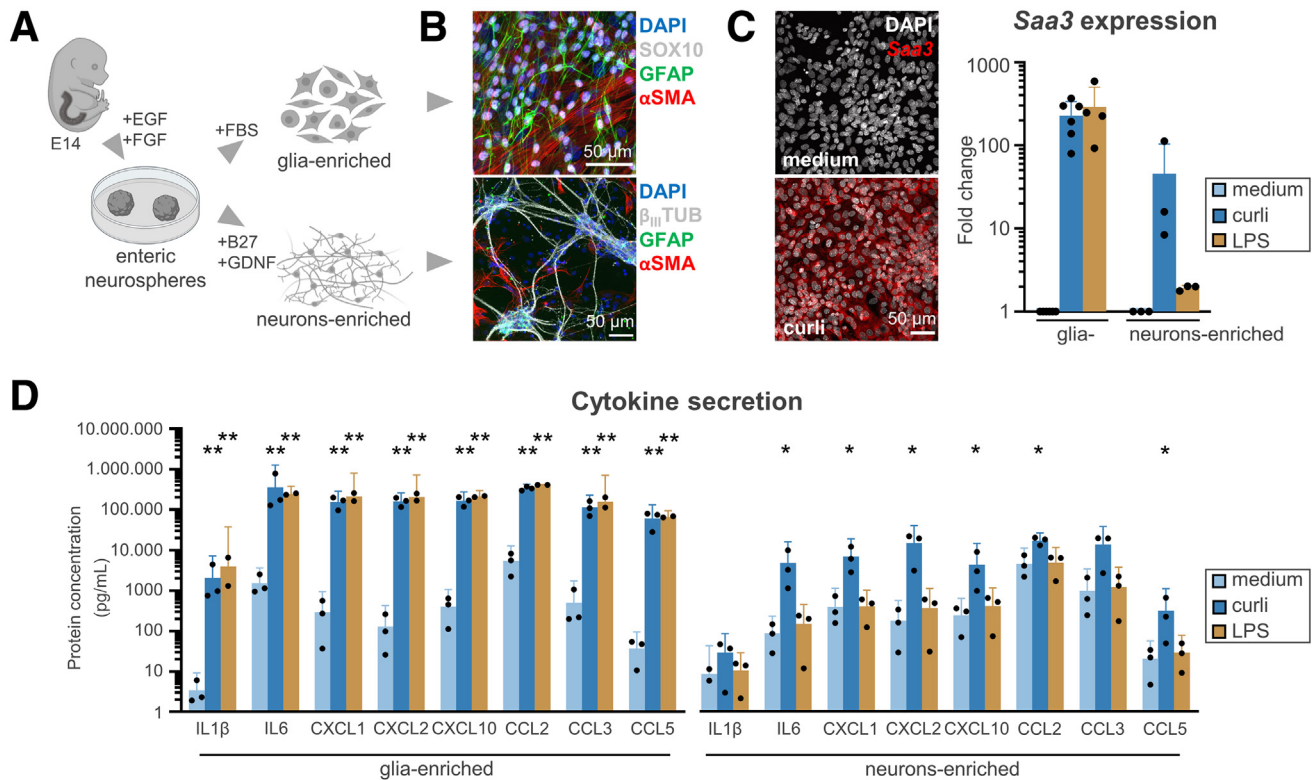


**Figure 2. Enteric glia are an important source of a curli-induced immune response.** (A) Experimental workflow for preparing glia- and neuron-enriched cultures, starting from embryonic enteric neurospheres. (B) Microscopic images showing glia (SOX10<sup>+</sup>/glial fibrillary acidic protein [GFAP]<sup>+</sup>) and smooth muscle cells ( $\alpha$ -smooth muscle actin [ $\alpha$ -SMA]<sup>+</sup>) in glia-enriched cultures, and neurons ( $\beta_{III}$ -tubulin), as well as a smaller number of glia and smooth muscle cells in neuron-enriched cultures. (C) *Saa3* mRNA was induced in glia- and to a lesser extent in neuron-enriched cultures upon 24-hour stimulation with curli, as shown by fluorescence in situ hybridization (left, glia-enriched cultures) and qPCR (right). LPS induced *Saa3* in glia- but not neuron-enriched cultures. Means + SD; n = 6 for glia- and n = 3 for neuron-enriched cultures. (D) Cytokine concentrations in the culture medium as measured with multiplex ELISA. Means + SD; n = 3 independent cultures; 2-way analysis of variance on log-transformed data per cell type: treatment  $P < .005$ , analyte  $P < .005$ , analyte\*treatment  $P < .005$ ; \* $P < .05$  and \*\* $P < .005$  in Dunnett post-hoc test with medium as the control level. DAPI, 4',6-diamidino-2-phenylindole; EGF, epidermal growth factor; FBS, fetal bovine serum; FGF, fibroblast growth factor; GFAP, glial fibrillary acidic protein; IL, interleukin;  $\beta_{III}$ -TUB,  $\beta_{III}$ -tubulin.

we found significantly more EdU<sup>+</sup> and EdU<sup>+</sup>/SOX10<sup>+</sup> nuclei, suggesting an extension of the replication window or a general increase in replication among these cells. Furthermore, we noticed that  $\gamma$ H2AX spots specifically accumulated in EdU<sup>+</sup> nuclei in control (medium-treated) cultures, and that curli further increased the abundance of  $\gamma$ H2AX<sup>+</sup>/EdU<sup>+</sup> nuclei, suggesting that cells undergoing replication were particularly vulnerable to DNA damage (Figure 3B and E). Under the experimental conditions used, curli proved to be as potent as LPS in inducing DNA damage and replication (Figure 3C-E). Together, these experiments show that in addition to the proinflammatory response, ENS cells activate replication and accumulate DNA damage in response to bacterial amyloid.

### Curli Injection in the Colon Wall Triggers DNA Damage, Cytokine Up-Regulation, and Immune Cell Infiltration

Having established that curli induces an inflammatory response *in vitro*, we next asked whether this effect would

be recapitulated in an *in vivo* context. As a direct means to expose the ENS, we performed curli injections in the proximal colon wall of live mice and prepared myenteric whole mounts from the region encompassing the injection site (Figure 4A). Herein, we observed several  $\gamma$ H2AX<sup>+</sup> nuclei 3 days after injection, which increased further 7 days after injection (Figure 4B). The accumulation of  $\gamma$ H2AX<sup>+</sup> nuclei was induced by curli but not by the control injection with PBS, and at 7 days after injection, nuclei showed punctate or diffuse pan-nuclear  $\gamma$ H2AX patterns (Figure 4B). After *in vivo* curli injection, we found a strong up-regulation in the myenteric plexus of *Cxcl2* and *Saa3* transcripts as measured by fluorescence in situ hybridization (Figure 4C). This was performed 4 hours after the injection to target the resident ENS cells only. Although *Cxcl2* mRNA localized predominantly to SOX10<sup>+</sup> glial nuclei (Figure 4C, arrowheads), *Saa3* was expressed by more diverse cell types, including enteric glia (Figure 4C, arrowheads). We next measured peripheral immune cell influx in curli-injected colon by flow cytometry, and observed increased CD45<sup>+</sup> immune cell counts in the muscularis 7 days after injection

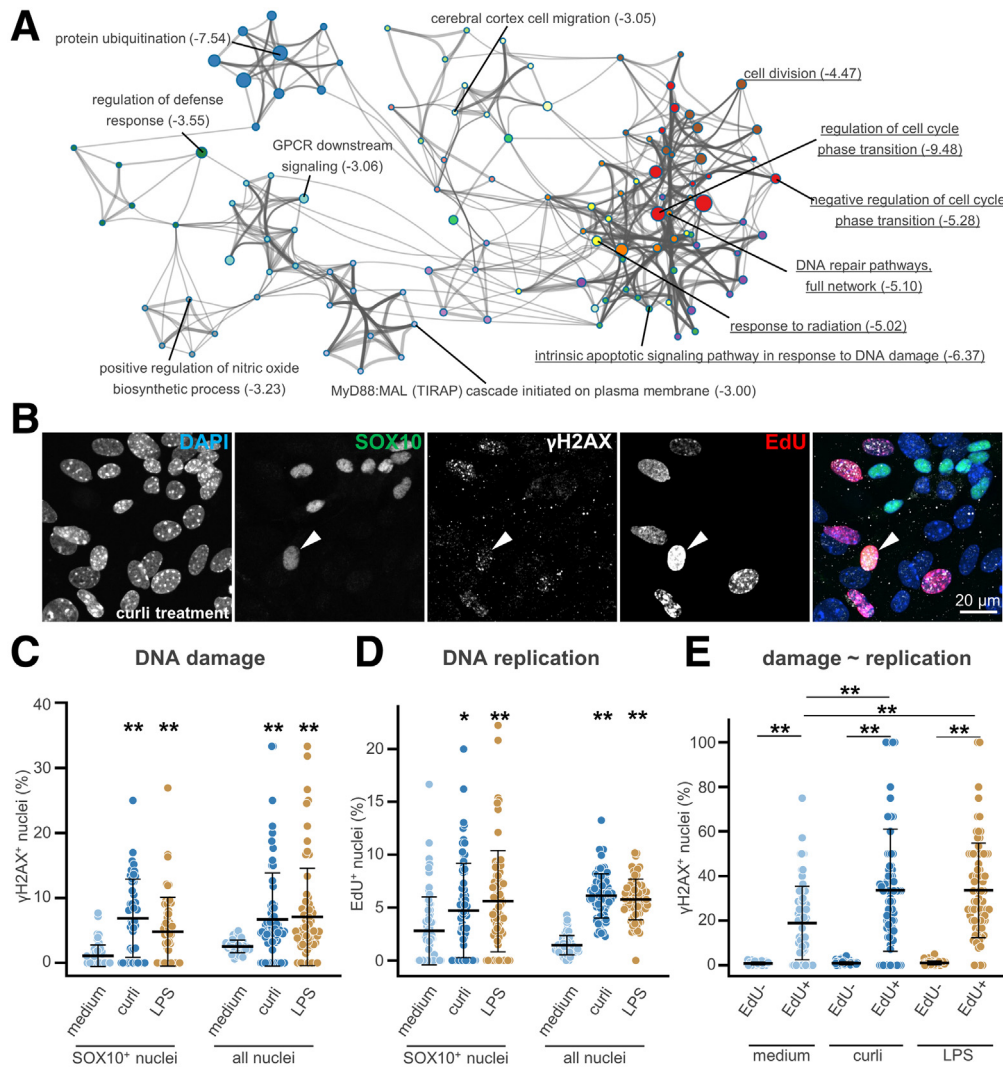


**Figure 3. Bacterial amyloid induces DNA damage and replication in vitro.** (A) Network plot of enriched Gene Ontology terms, colored by cluster and labeled with the most significant term and its log<sub>10</sub> P value between parentheses. Curli-provoked cell-cycle changes and DNA damage (relevant terms are *underlined*). (B) Microscopic image of a glia-enriched culture, stained for 4',6-diamidino-2-phenylindole (DAPI) (all nuclei), SOX10 (glial nuclei),  $\gamma$ H2AX (DNA damage spots), and EdU (DNA replication). The *arrowhead* indicates a SOX10<sup>+</sup>/EdU<sup>+</sup>/ $\gamma$ H2AX<sup>+</sup> nucleus. (C) The proportion of  $\gamma$ H2AX-positive nuclei, defined as nuclei with  $\geq 5$   $\gamma$ H2AX spots, increased in glial nuclei (SOX10 segmentation) and in all nuclei (DAPI segmentation) after 24 hours of exposure to curli or LPS. Means  $\pm$  SD; n = 3 independent cultures with 24 images/culture; analysis of variance (ANOVA) per segmentation type  $P < .005$ ;  $**P < .005$  in Dunnett with medium. (D) Quantification of the proportion of EdU<sup>+</sup> nuclei after SOX10 (glia) and DAPI (all cells) segmentation. Enteric glia-enriched cultures show increased EdU incorporation 24 hours after curli or LPS stimulation (EdU administered at the last 4 hours of curli/LPS exposure). Means  $\pm$  SD; n = 3 independent cultures with 24 images/culture; ANOVA per segmentation type  $P < .005$ ;  $*P < .05$   $**P < .005$  in Dunnett with medium. (E) Quantification of the percentage of  $\gamma$ H2AX<sup>+</sup> nuclei (after DAPI segmentation), stratified by EdU positivity (curli/LPS and EdU were administered simultaneously for only 4 hours). Means  $\pm$  SD; n = 2 independent cultures with 40 images/culture; 2-way ANOVA treatment  $P < .005$ , EdU  $P < .005$ , treatment\*EdU  $P < .005$ ;  $**P < .005$  in Tukey across all conditions. GPCR, G-protein coupled receptor; TIRAP, TIR domain containing adaptor protein.

(Figure 4D). Refining the molecular characterization, we found that curli injection specifically increased the infiltration of a CD45<sup>+</sup>CD3<sup>+</sup>TCR $\beta$ <sup>+</sup> T-cell population (Figure 4D). Collectively, these data show that curli induces DNA damage and local inflammation near the ENS in vivo. This inflammatory state is at least in part mediated by enteric glia and accompanied by sustained peripheral immune cell infiltration.

### Serum Amyloid A3 (SAA3) Mediates Curli Toxicity in Glia-Enriched Cultures

Because *Saa3* was among the highest up-regulated transcripts in both *in vitro* models after curli challenge (Figures 1C and 2C), as well as after *in vivo* curli injection (Figure 4C), and because SAA3 protein may behave as an amyloid,<sup>14,15</sup> we next asked whether SAA3 mediates the observed curli-induced inflammation. We therefore

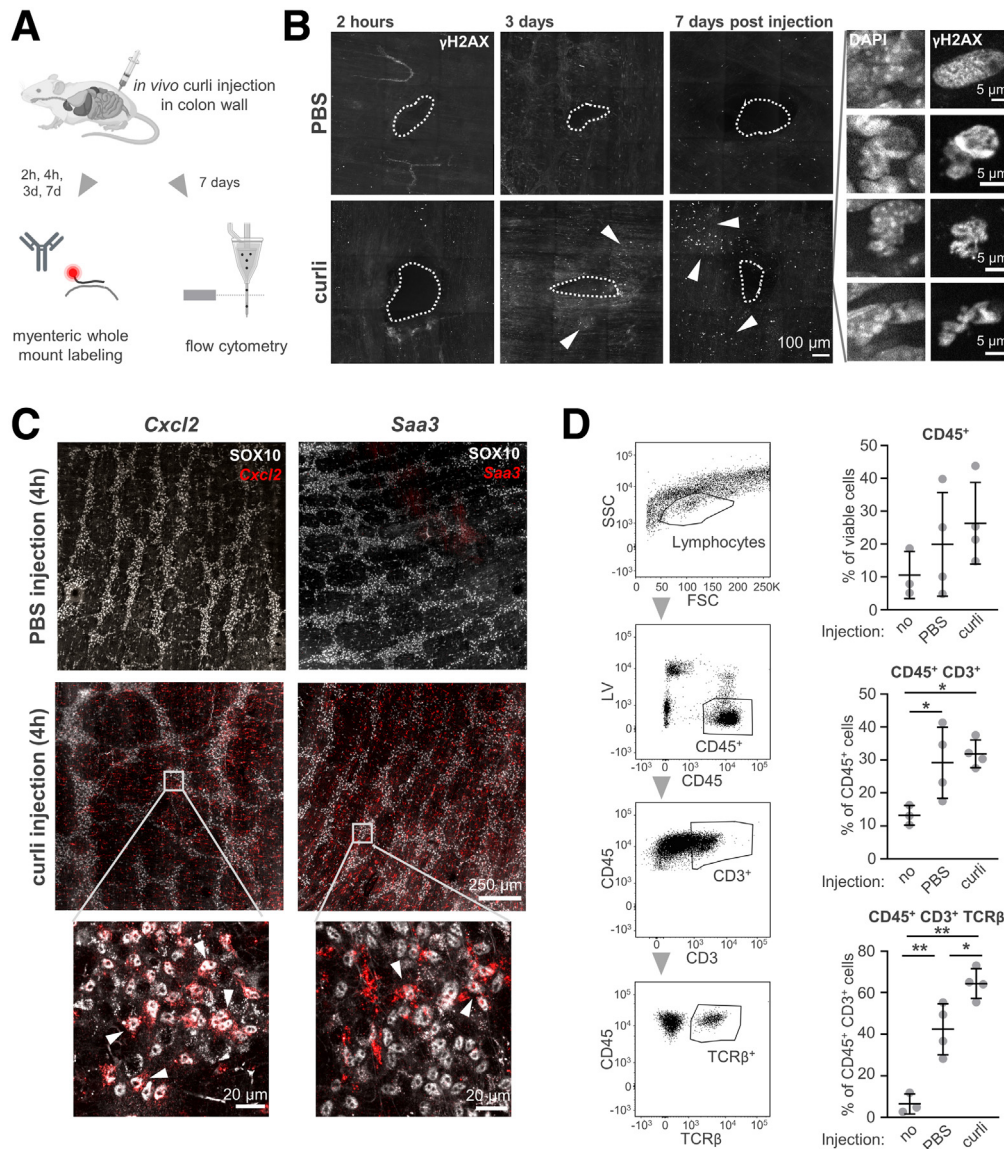


**Figure 4. Curli injection in the colon wall triggers DNA damage, cytokine up-regulation, and immune cell infiltration.** (A) Experimental workflow for quantifying phenotypic changes and immune cell infiltration after curli injection into the colon wall of live mice. (B) Curli but not PBS injection induced a time-dependent accumulation of  $\gamma$ H2AX<sup>+</sup> nuclei (arrowheads) in myenteric whole mounts (injection site indicated with a dotted line). Seven days after the injection,  $\gamma$ H2AX<sup>+</sup> nuclei showed a punctuate or pan-neuronal staining with nuclear deformations, reminiscent of cell death. (C) Fluorescence in situ hybridization shows that curli but not PBS induced *Cxcl2* and *Saa3* mRNA in the myenteric plexus, 4 hours after injection. *Cxcl2* is highly enriched in SOX10<sup>+</sup> enteric glia, whereas *Saa3* mRNA also is present in other cell types (arrowheads show *Cxcl2* or *Saa3* signal associated with SOX10<sup>+</sup> glial nuclei). (D) Sterile PBS or curli were injected in the proximal colon of live mice, and muscularis tissue of the colon was processed for flow cytometry 7 days later. A control group that did not undergo surgery was included as well. The injected animals show a trend toward higher CD45<sup>+</sup> immune cell influx. A population of T cells (CD45<sup>+</sup>CD3<sup>+</sup>TCR $\beta$ <sup>+</sup>) was specifically enriched after curli compared with PBS injection. Means  $\pm$  SD; n = 4 mice; analysis of variance CD45<sup>+</sup>  $P = .3243$ , CD45<sup>+</sup>CD3<sup>+</sup>  $P = .0224$ , CD45<sup>+</sup>CD3<sup>+</sup>TCR $\beta$ <sup>+</sup>  $P < .005$ ; \* $P < .05$  and \*\* $P < .005$  in post hoc test with Tukey correction. DAPI, 4',6-diamidino-2-phenylindole; LV, Live-Dead; SSC, sideward scatter.

challenged enteric glia-enriched cultures with mouse recombinant SAA3 protein (rSAA3) and measured cytokine gene expression by qPCR. rSAA3 treatment up-regulated the same cytokine panel as curli did (Figure 5A), and, interestingly, it also caused a significant up-regulation of *Saa3* itself. This indicates that SAA3 initiates a feedforward loop. Sole exposure to rSAA3 was sufficient to dose-dependently increase DNA damage (as measured by the proportion of

$\gamma$ H2AX<sup>+</sup> nuclei) (Figure 5B) and trigger DNA replication (as measured by EdU incorporation) (Figure 5C) in otherwise unperturbed cultures. Furthermore, rSAA3 treatment exacerbated curli-induced effects, underscoring its amplification potential (Figure 5B and C). To prove that SAA3 mediates the observed curli-induced pathogenic effects, we prepared glia-enriched cultures from *Saa3*<sup>lox/lox</sup>  $\times$  Cre<sup>ERT2</sup> mice. As anticipated, Cre-induced recombination of exon 3 drastically

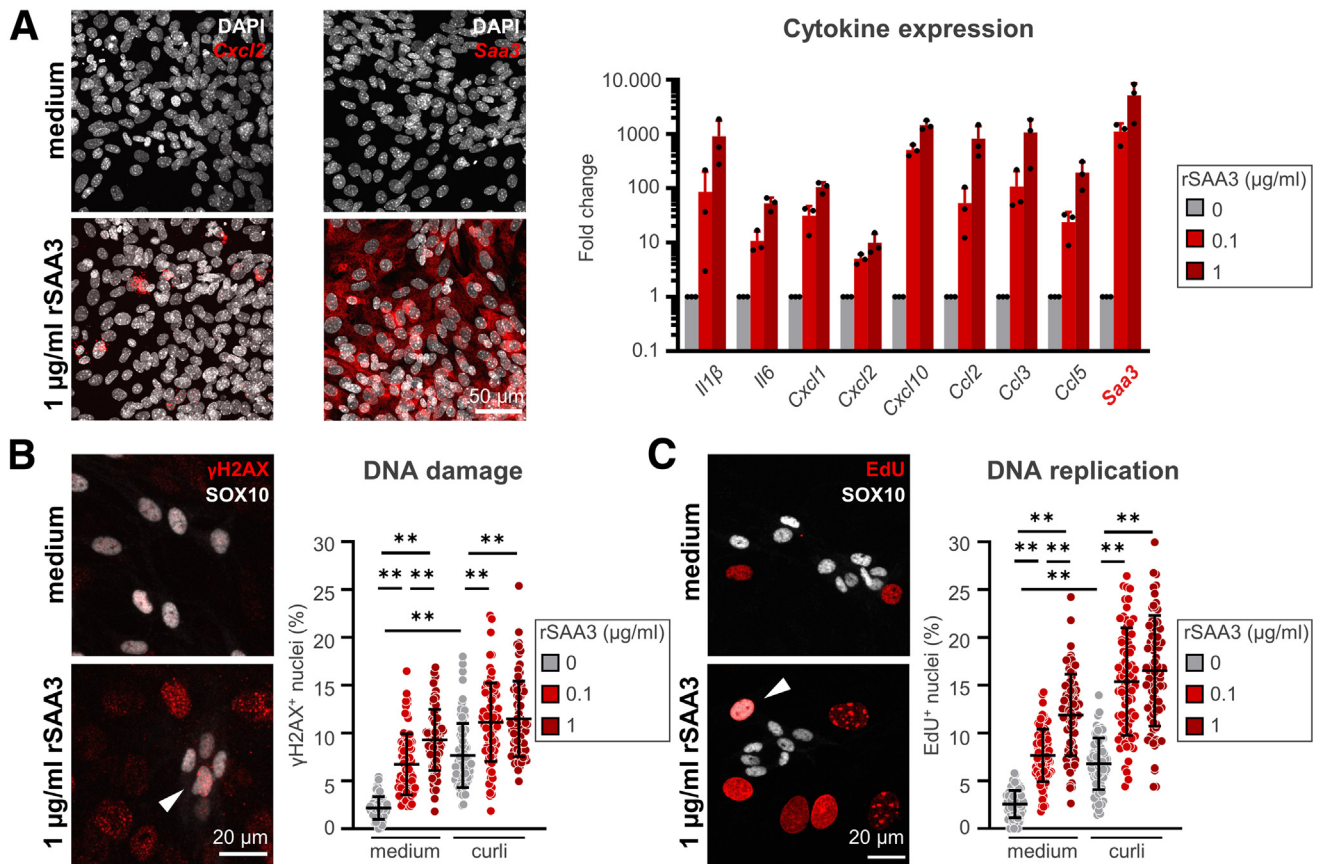


**Figure 5. Recombinant SAA3 recapitulates and potentiates curli-induced pathogenic effects.** (A) Glia-enriched cultures were challenged with mouse rSAA3 and gene expression was analyzed 24 hours later with fluorescence in situ hybridization (*left*) and qPCR (*right*). rSAA3 induced the same panel of proinflammatory cytokines, including *Saa3*, as previously seen after amyloid stimulation. Means + SD;  $n = 3$  independent cultures. (B) Glia-enriched cultures were exposed to rSAA3, 4 hours before curli (28-hour rSAA3 and 24-hour curli exposure in total). rSAA3 treatment induced  $\gamma$ H2AX spots in glia-enriched cultures and exacerbated curli-induced effects. The *arrowhead* indicates a SOX10<sup>+</sup>/ $\gamma$ H2AX<sup>+</sup> nucleus; 4',6-diamidino-2-phenylindole (DAPI) segmentation; means  $\pm$  SD;  $n = 3$  independent cultures with 40 images/culture; 2-way analysis of variance (ANOVA) rSAA3  $P < .005$ , curli  $P < .005$ , rSAA3\*curli  $P < .005$ ; \*\* $P < .005$  in Tukey across all conditions. (C) rSAA3 induced DNA replication, detected as a higher proportion of EdU<sup>+</sup> nuclei (the *arrowhead* indicates a SOX10<sup>+</sup>/EdU<sup>+</sup> nucleus), and exacerbated curli-induced replication. DAPI segmentation; means  $\pm$  SD;  $n = 3$  independent cultures with 40 images/culture; 2-way ANOVA rSAA3  $P < .005$ , curli  $P < .005$ , rSAA3\*curli  $P < .005$ ; \*\* $P < .005$  in Tukey across all conditions.

reduced curli-induced *Saa3* expression (Figure 6A). The proportion of  $\gamma$ H2AX<sup>+</sup> nuclei, induced by 0.1 or 1  $\mu$ g/mL curli, was attenuated significantly upon reduced *Saa3* expression (Figure 6B). Likewise, *Saa3* knockout cultures displayed a lower proportion of replicating (EdU<sup>+</sup>) nuclei when confronted with curli (Figure 6C). Collectively, these experiments indicate that (r)SAA3 can produce and potentiate pathogenic effects similar to those observed in curli-treated enteric glia.

### *Saa3* Becomes Up-Regulated in Multiple In Vivo Models of Intestinal Pathology

Having shown that SAA3 mediates curli toxicity *in vitro*, and becomes up-regulated after direct curli injection *in vivo*, we asked whether systemic exposure to curli would evoke the same response. To do so, we performed intraperitoneal

injections with purified curli fibrils and isolated RNA from colon homogenates 24 hours later (Figure 7A). We measured a strong induction of *Saa3* messenger RNA (mRNA) compared with a phosphate-buffered saline (PBS) injection, confirming that curli triggers *Saa3* production in the GI tract. Considering that some bacteria are potent curli producers, we next inoculated wild-type (WT) mice with *Salmonella enterica* serovar Typhimurium, a curli-producing bacterium responsible for GI infections. Forty-eight hours after inoculation, this treatment triggered significant *Saa3* expression compared with mice inoculated with lysogeny broth (LB) only (Figure 7B). Triggered by these observations, we wondered whether *Saa3* also would be upregulated in a more general condition of inflammation as well. Hence, we induced colitis by supplementing the drinking water with 2.5% dextran sulfate sodium (DSS), a substance that damages the epithelium after which the

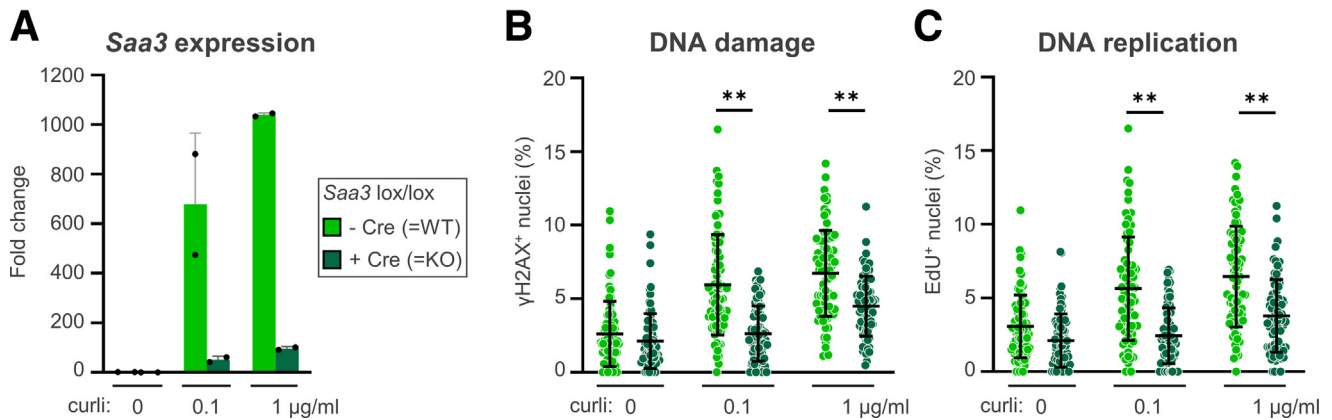


**Figure 6. Saa3 knockdown attenuates curli-induced pathogenic effects.** Glia-enriched cultures were prepared from  $Saa3^{lox/lox} \times Cre^{ERT2}$  embryos. (A) Cre-induced *Saa3* recombination attenuated curli-induced *Saa3* up-regulation. Means  $\pm$  SD;  $n = 2$  independent cultures. (B) The proportion of curli-induced  $\gamma$ H2AX<sup>+</sup> nuclei was attenuated in the absence of *Saa3* (4',6-diamidino-2-phenylindole [DAPI] segmentation). Means  $\pm$  SD;  $n = 2$  independent cultures with 40 images/culture; 2-way analysis of variance (ANOVA) curli  $P < .005$ , Cre  $P < .005$ , curli\*Cre  $P < .005$ ; \*\* $P < .005$  in  $t$  test with Sidak correction. (C) The proportion of curli-induced EdU<sup>+</sup> nuclei was attenuated in the absence of *Saa3* (DAPI segmentation). Means  $\pm$  SD;  $n = 2$  independent cultures with 40 images/culture; 2-way ANOVA curli  $P < .005$ , Cre  $P < .005$ , curli\*Cre  $P < .005$ ; \*\* $P < .005$  in  $t$  test with Sidak correction. KO, knockout.

luminal content activates the underlying immune system (Figure 7C). *Saa3* mRNA was enriched in colon homogenates of mice experiencing active colitis (killed 3 days after the last DSS exposure), compared with those that received normal drinking water. Together, these in vivo experiments showed that SAA3 constitutes a broad-spectrum mediator of GI inflammation.

### The c-Jun N-Terminal Kinase Pathway Governs the Curli- and rSAA3-Induced Cell Response

Because the c-Jun N-terminal Kinase (JNK) pathway is known for mediating cell responses to extracellular insults

and for regulating SAA3 secretion,<sup>16–18</sup> we tested whether its inhibition would reduce curli-mediated toxicity. To this end, we used GNE-3511, a validated inhibitor of dual leucine zipper kinase (DLK), a central regulator of the JNK pathway.<sup>19,20</sup> We found that JNK protein levels increased upon 24-hour curli challenge, but that GNE-3511 pretreatment (4 + 24 hours) dose-dependently prevented this increase (Figure 8A). The same pattern was observed for *Saa3* and *Ccl2*, in which curli induced their transcription but GNE-3511 blunted their up-regulation (Figure 8B). The expression of other cytokine genes was less affected. Importantly, GNE-3511 treatment also reduced curli-induced DNA

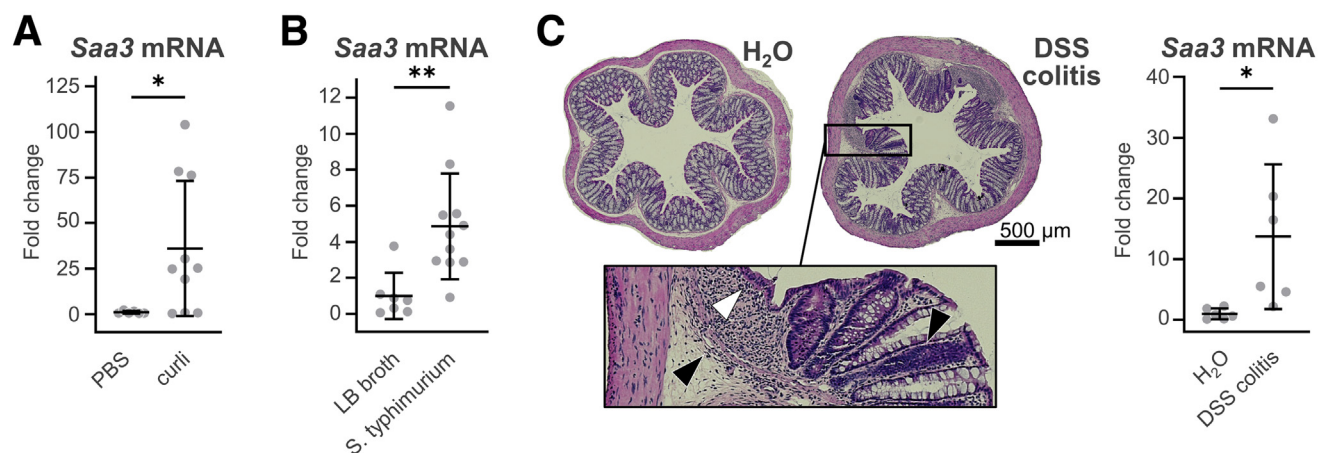


**Figure 7. Saa3 becomes up-regulated in multiple in vivo models of intestinal pathology.** (A) Intraperitoneal injection of 100 µg curli in WT C57BL/6 mice induced *Saa3* mRNA in the colon, 24 hours after injection. Means  $\pm$  SD;  $n = 10$  mice; \* $P < .05$  in Welch's  $t$  test for unequal variances. (B) Colonization of C57BL/6N mice with WT *S enterica* serovar Typhimurium for 48 hours induced *Saa3* up-regulation in colon homogenates compared with mice inoculated with lysogeny broth (LB) only. Means  $\pm$  SD;  $n \geq 7$  mice; \*\* $P < .005$  in Welch's  $t$  test. (C) Colon inflammation was induced in 9-month-old C57BL/6N mice by supplementing drinking water with 2.5% DSS for 7 days. This resulted in erosion of the mucosa (white arrowhead) and (sub-) mucosal cell infiltrates (black arrowheads), 3 days after cessation of DSS. *Saa3* transcripts were up-regulated significantly compared with the water control group. Means  $\pm$  SD;  $n = 6$  mice; \* $P < .05$  in Welch's  $t$  test.

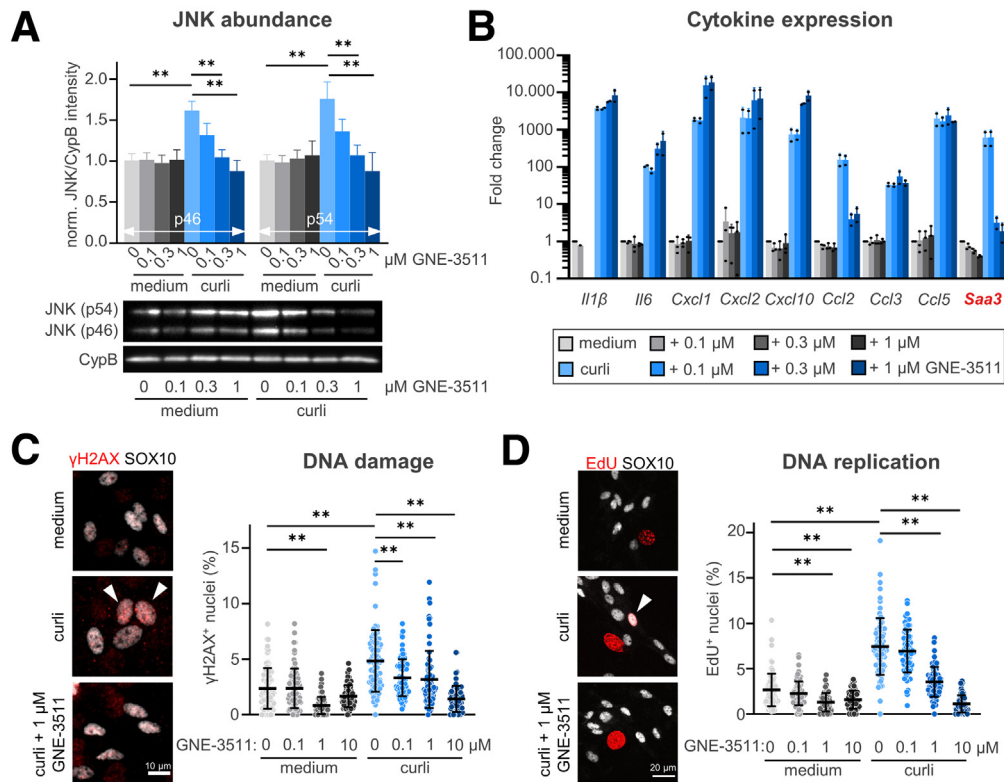


**Figure 8. The JNK pathway governs the curli-induced cell response.** Glia-enriched cultures were incubated with different concentrations of the DLK inhibitor GNE-3511 for 4 hours, before curli was added for 24 hours (28 hours of GNE-3511 exposure). (A) Western blot analysis shows increased DLK abundance (with p46 and p54 isoforms) upon curli stimulation, that was attenuated dose-dependently by GNE-3511 pretreatment. Means  $\pm$  SD,  $n = 3$  independent cultures; analysis of variance (ANOVA) p46: curli  $P < .005$ , DLK  $P < .005$ , curli\*DLK  $P < .005$  and p54: curli  $P < .005$ , DLK  $P < .005$ , curli\*DLK  $P < .005$ ; \*\* $P < .005$  in Tukey across all conditions. (B) GNE-3511 prevented curli-induced *Saa3* up-regulation, as measured with qPCR. Means  $\pm$  SD;  $n = 3$  independent cultures. (C) GNE-3511 prevented curli-induced DNA damage as measured by the proportion of  $\gamma\text{H2AX}^+$  nuclei (4',6-diamidino-2-phenylindole [DAPI] segmentation). Means  $\pm$  SD;  $n = 2$  independent cultures with 40 images/culture; 2-way ANOVA curli  $P < .005$ , GNE  $P < .005$ , curli\*GNE  $P < .005$ ; \*\* $P < .005$  in Tukey across all conditions. (D) GNE-3511 prevented curli-induced replication as measured by the proportion of EdU $^+$  nuclei (DAPI segmentation). Means  $\pm$  SD;  $n = 2$  independent cultures with 40 images/culture; 2-way ANOVA curli  $P < .005$ , GNE  $P < .005$ , curli\*GNE  $P < .005$ ; \*\* $P < .005$  in Tukey across all conditions. CypB, cyclophilin B; norm., normalized.

damage (Figure 8C) and replication (Figure 8D) in a dose-dependent manner. Thus, DLK inhibition proved to reverse curli-mediated pathogenic effects in glia-enriched cultures. Given that curli and rSAA3 triggered *Saa3* expression through a feedforward mechanism, we asked whether the JNK pathway also would mediate the effects induced by SAA3 protein in the absence of curli. In line with our previous data (Figure 5A), 24-hour rSAA3 treatment induced a dose-dependent up-regulation of all tested cytokines (Figure 9A). Furthermore, GNE-3511 pretreatment (4 + 24 hours) blunted the rSAA3-induced expression of several cytokines (*Il1 $\beta$* , *Il6*, *Cxcl1/2/10*, *Ccl2/3*, and *Saa3*), an effect that was most pronounced for the lower rSAA3 concentration (0.1  $\mu\text{g}/\text{mL}$ ), suggesting saturation of cytokine transcription at the higher rSAA3 concentration (1  $\mu\text{g}/\text{mL}$ ) (Figure 9A). A similar observation was made for DNA damage (Figure 9B) and replication (Figure 9C), in which rSAA3 induced a dose-dependent increase and GNE-3511 proved more effective at the lower rSAA3 concentration. These data confirm that rSAA3 induced a similar cellular

response as seen for curli and show that DLK inhibition dampens DNA damage and replication.

## Discussion

This study showed that the archetypical bacterial amyloid, curli, is not inert but activates pathogenic pathways in the host's GI tract. Using 3 different model systems (primary myenteric networks, enteric neurosphere-derived cultures, and in vivo injections), we have shown that the ENS launched a proinflammatory response when confronted with curli. Enteric glia clearly contributed to the proinflammatory environment, although we cannot rule out that other cells such as ganglia-associated macrophages reacted as well. The response was typified by secretion of cytokines, which are involved in chemotactic signaling and activation of the adaptive immune system. Seven days after the injection of curli into the colon wall, we noted the enrichment of a subset of reactive T cells, consistent with our finding that cultured glia released CCL5 and CXCL10, well-known

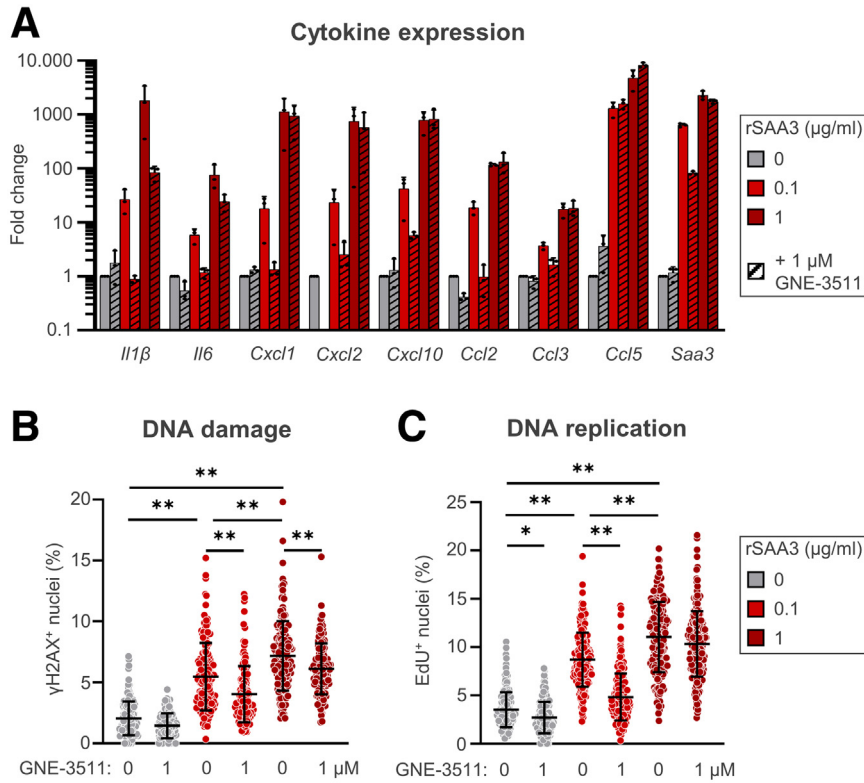


**Figure 9. DLK inhibition attenuates the rSAA3-induced cell response.** Glia-enriched cultures were incubated with 1  $\mu$ mol/L GNE-3511 for 4 hours, followed by rSAA3 addition for 24 hours (ie, 28 hours of GNE-3511 exposure). (A) GNE-3511 prevented rSAA3-induced cytokine expression, notably at the lower rSAA3 concentration of 0.1  $\mu$ g/mL. Means  $\pm$  SD; n = 3 independent cultures. (B) GNE-3511 prevented rSAA3-induced DNA damage as measured by the proportion of  $\gamma$ H2AX<sup>+</sup> nuclei after 4',6-diamidino-2-phenylindole (DAPI) segmentation. Means  $\pm$  SD; n = 3 independent cultures with 40 images/culture; 2-way analysis of variance (ANOVA) rSAA3  $P < .005$ , GNE  $P < .005$ , rSAA3\*GNE  $P = .053$ ; \*\* $P < .005$  in Tukey across all conditions. (C) GNE-3511 prevented rSAA3-induced DNA replication (EdU incorporation) at the lower rSAA3 concentration. Means  $\pm$  SD; n = 3 independent cultures with 40 images/culture; 2-way ANOVA rSAA3  $P < .005$ , GNE  $P < .005$ , rSAA3\*GNE  $P < .005$ ; \* $P < .05$  and \*\* $P < .005$  in Tukey across all conditions.

T-cell attractants. In addition to the inflammatory response, our data showed a previously unknown effect of curli on the cell cycle, which also was accompanied by a DNA damage response. In glia-enriched cultures, double-stranded DNA breaks ( $\gamma$ H2AX spots) accumulated preferentially in replicating (EdU<sup>+</sup>) cells, suggesting that these cells were more susceptible to curli-induced DNA damage during replication. However, because  $\gamma$ H2AX also enriched in EdU<sup>+</sup> cells at steady state, we cannot rule out that the observed increase in DNA damage was a direct consequence of the enhanced replication. Yet, also after *in vivo* curli injection, the number of  $\gamma$ H2AX<sup>+</sup> cells increased, which warrants further investigation into the genotoxic mechanisms and their functional consequences. Because enteric glial cells are known to regulate intestinal motility,<sup>21</sup> we speculate that their dysfunction may contribute to the gastrointestinal comorbidities observed commonly in dementia patients.<sup>22</sup>

Our experiments have shown that the acute-phase protein SAA3 plays a central role in amyloid-induced toxicity in the ENS. Not only was its expression consistently induced after curli challenge, exposure to rSAA3 also induced the same cytokines and phenotypic alterations as curli. Moreover, rSAA3 exacerbated curli-induced effects, which is consistent with the notion that SAA proteins behave as amyloids that aggregate<sup>14,23</sup> and signal through TLRs.<sup>15,24</sup> This, together with attenuation of curli-induced effects in *Saa3* KO cultures and up-regulation of *Saa3* mRNA after rSAA3 stimulation, suggests that local SAA3 production is at the center of a feedforward mechanism that sustains curli-induced enteric pathology. Besides direct curli injection, *Saa3* mRNA also was

increased after *Salmonella*-induced colitis. Compared with the intraperitoneal model, the up-regulation was less overt, plausibly because the ENS in WT mice is shielded by an intact intestinal epithelial barrier. Although certain studies have indicated a decline in barrier integrity upon aging<sup>25</sup> and inflammation,<sup>26</sup> ongoing debate remains regarding this topic, particularly concerning aging.<sup>27,28</sup> The colonization model suggests that the existence of curli-producing bacteria in the intestinal lumen may activate host immunity, even if the intestinal barrier remains unaffected by age or inflammation. In addition to these curli-oriented models, *Saa3* gene up-regulation was detected after DSS-induced colitis as well, underscoring the broad spectrum of enteric pathologies in which SAA3 serves as a mediator. Interestingly, SAA3 is found in the blood upon peripheral inflammation, bound to high-density lipoprotein.<sup>29</sup> Because of their lipophilic nature, SAA proteins can cross an intact blood-brain barrier. Although still speculative, SAA3 has the potential to transfer pathology over longer distances in the body, for example, from gut to brain. Furthermore, some studies have shown local *Saa3* expression in the central nervous system as well, more specifically in the hippocampus of aged WT and Amyloid Precursor Protein/Presenilin 1 (APP/PS1) mice,<sup>30</sup> and in microglia and monocyte-derived macrophages of the spinal cord during experimental autoimmune encephalomyelitis, where it sustains inflammation through a feedforward mechanism.<sup>31</sup> This suggests that SAA3 not only represents a mediator of amyloid toxicity and neuroinflammation in the ENS, but also in the central nervous system.

To alleviate the observed defects, we discovered that DLK inhibition prevents curli- as well as rSAA3-induced *Saa3* expression in the ENS, along with normalization of DNA damage accumulation and replication. This confirms the regulatory role of JNK in *Saa3* expression<sup>16–18</sup> and puts the JNK pathway upstream of the SAA3-mediated feedforward loop that is induced after curli exposure. The beneficial effects of the DLK inhibitor on curli- and rSAA3-induced DNA damage and replication seemed to be attained even in the presence of several proinflammatory cytokines (because their expression, apart from *Saa3*, was not always attenuated by the inhibitor). This may point to the pleiotropic nature of the DLK/JNK pathway in cell survival,<sup>19,20,32</sup> and warrants a further dissection of the molecular drivers. Nevertheless, its prominent activation in the brain of AD patients<sup>33</sup> and the gastrointestinal tract of inflammatory bowel disease patients<sup>34,35</sup> suggest that its selective targeting at different nodes along the gut–brain axis may represent a novel approach for treating amyloid-associated neurodegenerative disorders.

In sum, the current study shows the pathogenic potential of bacterial amyloids in the GI tract, and positions SAA3 as a mediator of the proinflammatory pathway. The impact of the curli–SAA3 axis on enteric and central neurodegeneration, as well as its functional implications, need to be studied further in a mouse model with prolonged curli exposure (eg, after chronic *Salmonella* colonization). Targeting the GI inflammatory state may open novel avenues for diagnosis and therapeutic intervention of amyloid-associated disorders in an early stage of the disease.

## Materials and Methods

### Mouse Lines and In Vivo Treatments

Wild-type C57BL6/N were bred and group-housed in the central animal facility at the University of Antwerp with food and water ad libitum and a dark/light cycle of 12/12 hours. To induce colitis, 9-month-old mice received 2.5% DSS via the drinking water for 7 consecutive days, followed by 3 days of normal drinking water before they were killed. Both male and female mice were used for the experiments, and all experimental procedures were approved by the Ethical Committee for Animal Testing of the University of Antwerp (file 2017-88).

The *Saa3* conditional knockout mouse model was generated at the Centro Nacional de Investigaciones Oncológicas (CNIO) Transgenics Unit (ethical file 257/19). Embryonic stem cells (G4; B6:129) were electroporated with the *Saa3* targeting vector (<https://www.komp.org>) and cultured in selection with G418. Ninety-six clones were analyzed by Southern blot (digestion with ApaI and hybridization with 5' and 3' probes external to the targeting vector), identifying 11 homologous recombinant clones. Next, the cassette flanked by the FRT sites was removed so that the conditional allele would be expressed normally until exon 3 (flanked by LoxP sites) in the absence of the Cre recombinase. Chimeras were generated, crossed for germline transmission of the conditional allele and for expansion of the line and generation of *Saa3*<sup>lox/lox</sup> mice. Embryonic day

14 (E14) mouse pups homozygous for *Saa3*<sup>lox/lox</sup> and heterozygous for Cre<sup>ERT2</sup> were obtained by mating a male, homozygous for *Saa3*<sup>lox/lox</sup> and Rosa26-Cre<sup>ERT2</sup>, with a female homozygous for *Saa3*<sup>lox/lox</sup>. This breeding scheme allowed pooling all pups for enteric neurosphere generation and obtaining *Saa3* knockout and control cultures from the same pool.

Microbial colonization and intraperitoneal curli injections were performed as previously described<sup>36,37</sup> in a biosafety level2 facility under protocols approved by AALAC-accredited Temple University Lewis Katz School of Medicine Institutional Animal Care and Use Committee (#4868) in accordance with guidelines set forth by the USDA and PHS Policy on the Humane Care and Use of Laboratory Animal Welfare. The institution has an Animal Welfare Assurance on file with the National Institutes of Health Office for the Protection of Research Risks, number A3594-01. At the age of 8 weeks, C57BL/6 mice received an intraperitoneal injection with 100  $\mu$ g fibrillar curli, and were killed 24 hours later to isolate the proximal colon for qPCR. Twenty-four hours before bacterial inoculation, mice received an intragastric gavage with 20 mg streptomycin in sterile water. They then were inoculated with 10<sup>8</sup> colony-forming units *Salmonella* Typhimurium IR715 or sterile LB broth, and killed 48 hours later.

### Curli Preparation

Curli fibrils were isolated from *Salmonella* Typhimurium as previously described.<sup>38</sup> These curli fibrils are produced in *msbB* mutant bacteria that express a modified LPS that does not signal through TLR4.<sup>8</sup> Additionally, there is an LPS stripping process at the end of curli purification to ensure that curli preparations are devoid of LPS. An aliquot of curli was thawed from  $-80^{\circ}\text{C}$ , dissolved to the desired concentration, bath sonicated, and used immediately. Low-binding Eppendorf tubes and filter tips were used to ascertain maximal recovery.

### Myenteric Network Isolation

Myenteric networks were isolated as described previously.<sup>39</sup> Briefly, animals were killed via cervical dislocation and exsanguination, after which the entire colon was removed and transferred to a dish containing ice-cold dissection buffer (Minimal Essential Medium (MEM) with GlutaMAX and HEPES [ThermoFisher 42360032] + 1% Penicillin and Streptomycin [Pen/Strep]). The mesentery was removed, and the colon was cut open along the mesentery line. The muscularis externa was stripped off with fine forceps under a binocular microscope, cut into small ( $\sim 25\text{ mm}^2$ ) pieces, and digested enzymatically (0.4 U Liberase [5401151001; Roche] and 60 U DNase I [A3778; AppliChem] in Hank's balanced salt solution–Ca–Mg, 37°C and 5% CO<sub>2</sub> for 4.5 hours without shaking). Remaining smooth muscle cells were removed mechanically by gentle pipetting under a binocular stereomicroscope until the space between the ganglia was devoid of cells. The cleaned networks were transferred to a 48-well plate (2 wells per mouse  $\times$  3 mouse replicates) with 250  $\mu$ L culture medium

(Dulbecco's modified Eagle medium [DMEM]-F12 with GlutaMAX [31331028; ThermoFisher], 2% B27 supplement [17504044; ThermoFisher], 1% bovine serum albumin, 0.1%  $\beta$ -mercaptoethanol, and 1% Pen/Strep). After an overnight recovery period, the networks were stimulated with 5  $\mu$ g/mL curli fibrils or nonsupplemented DMEM-F12 medium as a control. Twenty-four hours later, networks were lysed in RLT buffer + 1%  $\beta$ -mercaptoethanol for RNA isolation, and conditioned medium was collected for cytokine measurements with multiplex ELISA (U-Plex kit; Meso Scale Discovery).

### mRNA Sequencing

RNA was isolated using an RNeasy micro kit (Qiagen), its concentration was measured with a Qubit device (ThermoFisher), and the integrity was checked with a Bioanalyzer RNA pico chip (Agilent) (RNA Integrity Number >8). Complementary DNA (cDNA) libraries were prepared using a QuantSeq 3' mRNA-seq Library Prep kit FWD (Lexogen) and a qPCR add-on kit after which they were run on a Fragment Analyzer (Agilent), equimolar pooled, and sequenced using an Illumina NextSeq 500/550 High Output Kit v2.5 (75 cycles). Resulting reads were trimmed using the UrQt and SortMeRNA packages for R and aligned to the mouse reference genome (mm10) using Rsubread.<sup>40–42</sup> Differentially expressed genes were identified using DESeq2 with standard settings (Benjamini-Hochberg-adjusted *P* value cut-off at .1).<sup>43</sup> Volcano plots were made in GraphPad Prism 9. Functional annotation, including Gene Ontology term enrichment and construction of a network plot, were performed with Metascape using default settings.<sup>44,45</sup> A network plot was constructed in Cytoscape 3.10.0.<sup>46</sup>

### Neurosphere-Derived Enteric Glia- and Neuron-Enriched Cultures

Small and large intestines were dissected from E14 embryos and digested with 1 mg/mL DNase 1 (A3778; AppliChem) and 1 mg/mL collagenase A (10103586001; Merck Millipore) in DMEM-F12 at 37°C while shaking. After 45 minutes of digestion, samples were filtered through a 70- $\mu$ m cell strainer and cells were collected in DMEM-F12 medium supplemented with 1% GlutaMAX, 1% HEPES, 1% sodium pyruvate, and 1% Pen/Strep. They were centrifuged (5 minutes, 300  $\times$  *g*) and resuspended in DMEM-F12 medium supplemented additionally with 2% B27, 40 ng/mL epidermal growth factor (12343407; ImmunoTools), and 20 ng/mL fibroblast growth factor (12343627; ImmunoTools). Cell material of 1 embryo was divided over 2 wells of a 6-well plate, in a volume of 2 mL per well. Neurospheres were allowed to grow for 1 week whereby growth factors were replenished on days 3 and 5. For final plating, supernatant containing nonattached neurospheres was collected and centrifuged (5 minutes, 300 $\times$  *g*). Attached neurospheres were briefly trypsinized, added to the same tube, and again centrifuged (5 minutes, 300 $\times$  *g*). To obtain glia-enriched cultures, neurospheres were plated into 24- or 96-well plates in DMEM containing 10% fetal bovine serum, 1% GlutaMAX, 1% HEPES, 1%

sodium pyruvate, and 1% Pen/Strep. Glia-enriched cultures were used for experiments 5–7 days after final plating. To obtain neuronal cultures, neurospheres were plated onto Poly-D-Lysine-coated 24- or 96-well plates in Neurobasal medium (21103049; ThermoFisher) with 2% B27, 40 ng/mL glial cell line derived neurotrophic factor (512-GF-010; R&D Systems), 1% GlutaMAX, 1% HEPES, and 1% Pen/Strep. The neuronal network was allowed to grow for 7 days before experimental treatments were started. Curli fibrils (5  $\mu$ g/mL unless indicated otherwise), LPS from *E coli* (tlr1-3pelps, 100 ng/mL; InvivoGen), and mouse rSAA3 (0.1 or 1  $\mu$ g/mL, orb244746; biorbyt) were used to stimulate neurosphere-derived cultures. EdU (10  $\mu$ mol/L, C10338; ThermoFisher) was added 4 hours before fixation, and developed according to the manufacturer's instructions. A combination approach was optimized to induce *Saa3* knockout in glia-enriched cultures prepared from *Saa3*<sup>lox/lox</sup>  $\times$  *Cre*<sup>ERT2</sup> embryos. Twenty-four hours after final plating, cultures were transduced with AAV-DJ-CAG-iCre particles (plasmid #51904; Addgene; deposited by Jinhyun Kim, packaged in house with an AAV-DJ helper-free packaging kit, VPK-400-DJ; Cell Biolabs). Additionally, cultures were exposed to 4OH-tamoxifen (5  $\mu$ mol/L, 3412; Tocris) for a total time of 28 hours (3 $\times$  administered: 4 hours before curli, along with curli and with EdU). The combinatorial approach led to maximal knockdown with minimal toxicity at the time of analysis.

### Intramural Injections and Whole Mount Preparation

Mice were injected at the age of 12 weeks. Inhalation anesthesia was induced with 5% isoflurane and maintained with 2.5% isoflurane. Animals were shaved and the abdomen was washed with germicidal soap. The eyes were covered with an ophthalmologic gel and the animals were placed on a heating pad and covered with a sterile surgical cloth. A pre-emptive subcutaneous injection with 0.05 mg/kg buprenorphine was administered, after which the abdominal cavity was opened along the linea alba. The cecum was exteriorized and wetted regularly with physiological solution. Curli fibrils or sterile PBS were injected into the colon wall at 5 injection sites in a 1-cm region of the proximal colon. A total of 8  $\mu$ g in 5  $\times$  2  $\mu$ L was injected using a 35G NanoFill needle (World Precision Instruments). The region where the injections were given was marked by 2 final injections with tattoo ink. The abdominal muscles were closed fully by using a continuous suture with 5.0 resolvable thread. The skin then was closed using subcutaneous sutures with 5.0 silk thread. Finally, a subcutaneous injection with 0.05 mg/kg buprenorphine was given before animals were placed under a heating lamp for recovery. The animals were placed in separate cages and monitored closely. The next morning, a final subcutaneous injection with 0.05 mg/kg buprenorphine was given. Mice were killed by cervical dislocation, exactly 2 or 4 hours, or 3 or 7 days, after intramural injection. The proximal colon was dissected out and flushed with ice-cold Krebs solution. After removing the mesentery, the colon was opened along the mesentery

line and pinned open in a black Sylgard Petri dish and fixed with 4% paraformaldehyde (PFA) (2 hours at room temperature for immunostaining or 24 hours at 4°C for fluorescence in situ hybridization). Myenteric whole mounts were prepared by separating the external muscle layer from the submucosa/mucosa and removing the circular muscle layer under a stereomicroscope.

### Immunostaining and Microscopy

All immunostaining steps were performed in 96-well plates (50  $\mu$ L/well) for cell cultures and in 1.5-mL Eppendorf tubes (150  $\mu$ L/tube) at room temperature while gently shaking for whole mounts. Permeabilization was performed in blocking buffer (0.1% bovine serum albumin, 10% normal horse serum in PBS; Innovative Research IGHSSER) with 1% Triton X-100 (Sigma-Aldrich), for 5 minutes (cell cultures) or 2 hours (whole mounts). Primary antibodies (Table 1) were applied in blocking buffer for 4 hours (cultures) or 48 hours (whole mounts), followed by a PBS wash. Secondary antibodies (Table 1) were applied 2 hours (cell cultures) or overnight (whole mounts), followed by a 10-minute incubation with 4',6-diamidino-2-phenylindole (2.5  $\mu$ g/mL) and a final PBS wash. Whole mounts were cover slipped in Citifluor (17970-100; EMS) with the side of the myenteric plexus facing the cover glass. Multichannel Z-stacks were acquired on a spinning disk confocal microscope (UltraVIEW VoX, PerkinElmer) with 20 $\times$  air (numerical aperture [NA], 0.75) and 60 $\times$  oil (NA, 1.4) immersion objectives, or on a Nikon CSU-W1-SoRa spinning disk system with a 10 $\times$  air (NA, 0.45), 40 $\times$  air (NA, 0.95), or 100 $\times$  silicone (NA, 1.35) immersion objective. To obtain overview images of injection sites, 3  $\times$  3 tiles were recorded with 10% overlap followed by flatfield correction and stitching in Fiji freeware.<sup>47</sup> Segmentation and quantification of cell images (nuclei and  $\gamma$ H2AX spots) were performed with the FIJI script CellBlocks.<sup>48</sup>

### qPCR

Cells or colon segments were lysed in RLT buffer with 1%  $\beta$ -mercaptoethanol, and RNA was isolated via column purification (NucleoSpin RNA kit, 740955; Macherey-Nagel). RNA integrity and concentration were determined with BioAnalyzer (Agilent) and Nanodrop systems (Thermo Scientific), and 500 ng RNA (RIN, >8) was transcribed to cDNA using the iScript first-strand cDNA synthesis kit (1708891; Bio-Rad). qPCR was performed on a 384-well Quantstudio Flex system (ThermoFisher) using the SsoAdvanced Universal SYBR Green master mix (1725272; Bio-Rad) with 0.5  $\mu$ mol/L forward and reverse primers (Table 2) and a 1:10 dilution of the cDNA. The protocol comprised an initial 30-second denaturation step (95°C), followed by 40 cycles of 10 seconds at 95°C and 30 seconds at 60°C, and, finally, a melting curve. Fold change was calculated via the  $\delta\delta$ Ct method.

### Fluorescence In Situ Hybridization

Fluorescence in situ hybridization on whole mounts of the colonic myenteric plexus was performed using the Advanced Cell Diagnostics RNAscope Fluorescent Multiplex v2 Kit (323100; ACD) according to the manufacturer's instructions. After a 24-hour fixation with 4% PFA at 4°C, whole mounts were prepared and dehydrated through a graded ethanol series, followed by hydrogen peroxide treatment for 10 minutes at room temperature. Then, tissues underwent antigen retrieval for 5 minutes at 100°C, followed by Protease Plus treatment for 30 minutes at 40°C. The tissue was incubated with RNAscope probe (RNAscope probes 437581 Mm-Cxcl2 and 446841 Mm-Saa3) at 40°C under orbital shaking for 2 hours. After probe hybridization, whole mounts were washed twice with wash buffer and then processed for sequential amplification hybridizations using amplifier DNA (Amplifier 1, amplifier 2 and amplifier 3) at 40°C for 30, 30, and 15 minutes, respectively.

**Table 1.** Primary and Secondary Antibodies

Primary antibody	Species/clonality	Company and catalog number	Concentration
<b>Staining</b>			
$\alpha$ -smooth muscle actin-Cy3	Mouse monoclonal	Sigma C6198	1 $\mu$ g/mL
$\beta$ <sub>III</sub> -tubulin-Alexa Fluor 647	Mouse monoclonal	BioLegend 801210	1 $\mu$ g/mL
$\gamma$ H2AX	Rabbit polyclonal	Abcam ab2893	2 $\mu$ g/mL
GFAP	Goat polyclonal	Abcam ab53554	2 $\mu$ g/mL
SOX10	Goat polyclonal	Biotechnie AF2864	0.2 $\mu$ g/mL
<b>Flow cytometry</b>			
CD45-APC-eFluor780	Rat monoclonal	eBioscience 47-0451-82	0.5 $\mu$ g/mL
CD3e-PerCP-Cy5.5	Hamster monoclonal	eBioscience 45-0031-82	0.5 $\mu$ g/mL
TCR $\beta$ -APC	Hamster monoclonal	BioLegend 109211	0.5 $\mu$ g/mL
Ly6G-BV785	Rat monoclonal	BioLegend 12765	0.5 $\mu$ g/mL
<b>Secondary antibody</b>			
Donkey-anti-rabbit-Cy3		Jackson ImmunoResearch 711-165-152	2 $\mu$ g/mL
Goat-anti-rabbit Fab fragments-FITC		Jackson ImmunoResearch 111-097-003	1 $\mu$ g/mL
Donkey-anti-goat-FITC		Jackson ImmunoResearch 705-095-147	2 $\mu$ g/mL
Donkey-anti-goat-Cy3		Jackson ImmunoResearch 507-545-003	2 $\mu$ g/mL
Donkey-anti-goat-Alexa Fluor 647		Jackson ImmunoResearch 705-605-003	2 $\mu$ g/mL

APC, Allophycocyanin; Cy3, Cyanine3; Fab, antigen-binding; FITC, fluorescein; GFAP, glial fibrillary acidic protein; Ly6G, lymphocyte antigen 6 family member G; PerCP, Peridinin-Chlorophyll; TCR, T cell receptor  $\beta$  chain.

**Table 2.** Primers for qPCR

Gene	Forward primer	Reverse primer
<i>IL1<math>\beta</math></i>	TGCCACCTTTTGACAGTGATG	TGATGTGCTGCTGCGAGATT
<i>IL6</i>	CCATAGCTACCTGGAGTACATG	TGGAAATTGGGGTAGGAAGGAC
<i>Ccl2</i>	TGCCCTAAGGTCTTCAGCAC	AAGGCATCACAGTCCGAGTC
<i>Ccl3</i>	GCCACATCGAGGGACTCTTC	GATGGGGGTTGAGGAACGTG
<i>Ccl5</i>	GGAGATGAGCTAGGATAGAGGG	TGCCCATTTTCCCAGGACCG
<i>Cxcl1</i>	AAGGTGTCCCAAGTAACGG	TGTTGTGTCAGAAGCCAGCGTT
<i>Cxcl2</i>	GCTGTCCCTCAACGGAAGAA	CAGGTACGATCCAGGCTTCC
<i>Cxcl10</i>	TGAGAGACATCCCAGCCAA	GAGGCAGAAAATGACGGCAG
<i>Saa3</i>	CGCAGCACGAGCAGGAT	TGGCTGTCAACTCCCAGG
<i>Saa3_b</i>	GACATGTGGCGAGCCTACTC	TTGGCAAACCTGGTCAGCTCT
<i>eEF2</i>	TAAGGAGGGCGCTCTCTGTGAGG	TGGCCACCTCCCCGGTGAAT
<i>GAPDH</i>	TGAAGGTCGGTGTGAACGG	TGAAGGTCGGTGTGAACGG
<i>RPS29</i>	GCAAATACGGGCTGAACATG	GACTAGCATGATCGGTTCCAC

NOTE. *Saa3\_b* primers, targeting exons 3–4, were used exclusively to detect knockdown in cultures prepared from *Saa3<sup>lox/lox</sup> × Cre<sup>ERT2</sup>* embryos.

Fluorescent signal was developed with TSA Vivid Fluorophore 520 according to the manufacturer's instructions. After the RNAscope assay, tissues were counterstained with SOX10 and 4',6-diamidino-2-phenylindole, and mounted with ProLong Gold antifade reagent (P10144; ThermoFisher). For analysis on neurosphere-derived enteric glial cultures, all procedures were similar to those for colonic whole mounts, with some minor modifications according to the manufacturer's protocol. Specifically, fixation time was reduced to 30 minutes at room temperature, antigen retrieval was omitted, and protease treatment was performed with 1:15 diluted Protease Plus for 10 minutes at 40°C.

### Flow Cytometry

A 3-cm piece of the proximal colon, containing the 1-cm injected region, was isolated 7 days after injection. The muscularis was removed with fine forceps under a binocular stereomicroscope. Small tissue pieces were digested with 0.5 mg/mL collagenase D (11088882001; Roche) and 5 U/mL DNase 1 (10104159001; Sigma-Aldrich) in RPMI-1640 supplemented with 2% HEPES and 2% fetal bovine serum for 30 minutes at 37°C with continuous shaking. The resulting cell suspension was blocked using fluorescence-activated cell sorter (FACS) buffer and passed through a 70- $\mu$ m cell strainer, after which cells were centrifuged at 400  $\times$  *g* for 8 minutes at 4°C. Surface staining was performed by incubating cell suspensions for 20 minutes at 4°C with a mix of fluorescently conjugated antibodies (Table 1) in FACS buffer, followed by a PBS wash. To distinguish the live and dead cells, the cell pellets were resuspended in Live/Dead Fixable Aqua Dead Cell Strain kit solution (L34965; ThermoFisher) and incubated in the dark at room temperature for 30 minutes. Then, the cell pellets were fixed with 2% PFA at room temperature for 10 minutes, followed by a PBS wash and resuspension in FACS buffer. Data were

acquired using a FACSria II Cell Sorter (Becton Dickinson), and analyzed using FlowJo software (version 4.6.2; Treestar).

### Western Blot

Glia-enriched cultures were lysed using ice-cold RIPA buffer supplemented with phosphatase and protease inhibitor (HALT cocktail, 78445; ThermoFisher) and 5 mmol/L EDTA. The lysate was centrifuged (10,000  $\times$  *g*, 20 minutes, 4°C) and the protein concentration of the supernatant was determined using a bicinchoninic acid assay (23225; ThermoFisher). Samples were denatured (70% sample, 25% lithium dodecyl sulfate, 5% dithiothreitol) for 10 minutes at 70°C before being loaded on a 4–12% Bis-Tris gel (NP0322BOX; ThermoFisher) at 15  $\mu$ g/lane. A stained ruler was included in the first and last well (26616; ThermoFisher). The gel tank was filled with NuPage MOPS sodium dodecyl sulfate running buffer and NuPage anti-oxidant, and was cooled during electrophoresis (200 V,  $\pm$ 1 h). Proteins were transferred to a polyvinylidene difluoride membrane using NuPage transfer buffer (30 V, 1 h). Blots subsequently were blocked with 5% ECL blocking solution in Tris-buffered saline with 0.1% Tween (TBS-T). Primary antibody (rabbit anti-SAPK/JNK, 559304, 1  $\mu$ g/mL; Merck) was applied overnight at 4°C on a roller, followed by a TBS-T wash (3  $\times$  5 minutes). Horseradish-peroxidase-coupled goat-anti-rabbit was incubated for 2 hours at room temperature, followed by a final TBS-T wash. Bioluminescent detection was performed using Immobilon Western horseradish-peroxidase substrate (WBKLS0500, 30 seconds; Merck Millipore) and a Chemidoc Touch imager (BioRad). After completion, the blots were restained for cyclophilin B (ab16045, 0.2  $\mu$ g/mL; Abcam) as loading control. The mean intensity of the bands was measured with Fiji image analysis freeware and expressed as the intensity of the band of interest divided by the cyclophilin B intensity.

### Experimental Design

RNA-seq was performed on primary myenteric networks that were isolated from 3 mice. Material from each mouse was divided over 2 wells (for medium or curli treatment). Similarly, cytokine release was measured in myenteric networks from 8 mice, prepared on 2 different days and including the 3 mice that were used for RNA-seq. Microscopic analyses on neurosphere-derived cultures were performed on 2 wells with 20 images per well (1 data point = 1 image), originating from 2 or 3 independent cultures, that is, week-separated, neurosphere-derived cultures prepared from different mothers (E14 embryos were pooled). Likewise, multiplex ELISA, qPCR, and Western blot were performed on  $\geq 2$  independent cultures, as mentioned in the respective figure captions. For in vivo injections, 3 mouse replicates were considered for each treatment and time point, whereby 2 whole mounts could be prepared per mouse for different stainings/in situ hybridizations. Flow cytometry was performed on 4 mouse replicates per treatment type, and in vivo GI inflammation models (DSS, microbial colonization, intraperitoneal curli injection) were repeated on  $\geq 6$  mice. Graphing and statistical analyses were performed in GraphPad Prism 9 and SAS JMP Pro 14. The number of replicates and the nature and results of statistical analyses are reported in the figure captions. After parametric analyses, residuals were inspected visually for normality and homoscedasticity.

Schematic representations of experimental protocols were created with BioRender.

All authors had access to the study data and reviewed and approved the final manuscript.

### References

- Kim GH, Lee YC, Kim TJ, et al. Risk of neurodegenerative diseases in patients with inflammatory bowel disease: a nationwide population-based cohort study. *J Crohns Colitis* 2022;16:436–443.
- Zhang B, Wang HE, Bai Y-M, et al. Inflammatory bowel disease is associated with higher dementia risk: a nationwide longitudinal study. *Gut* 2021;70:85.
- Cryan JF, O’Riordan KJ, Sandhu K, et al. The gut microbiome in neurological disorders. *Lancet Neurol* 2020;19:179–194.
- Cattaneo A, Cattane N, Galluzzi S, et al. Association of brain amyloidosis with pro-inflammatory gut bacterial taxa and peripheral inflammation markers in cognitively impaired elderly. *Neurobiol Aging* 2017;49:60–68.
- Wallen ZD, Demirkan A, Twa G, et al. Metagenomics of Parkinson’s disease implicates the gut microbiome in multiple disease mechanisms. *Nat Commun* 2022;13:6958.
- Tytgat HLP, Nobrega FL, van der Oost J, et al. Bowel biofilms: tipping points between a healthy and compromised gut? *Trends Microbiol* 2019;27:17–25.
- Miller AL, Bessho S, Grando K, et al. Microbiome or infections: amyloid-containing biofilms as a trigger for complex human diseases. *Front Immunol* 2021;12:638867.
- Tükel C, Raffatellu M, Humphries AD, et al. CsgA is a pathogen-associated molecular pattern of *Salmonella enterica* serotype Typhimurium that is recognized by Toll-like receptor 2. *Mol Microbiol* 2005;58:289–304.
- Tükel C, Nishimori JH, Wilson RP, et al. Toll-like receptors 1 and 2 cooperatively mediate immune responses to curli, a common amyloid from enterobacterial biofilms. *Cell Microbiol* 2010;12:1495–1505.
- Tursi SA, Lee EY, Medeiros NJ, et al. Bacterial amyloid curli acts as a carrier for DNA to elicit an autoimmune response via TLR2 and TLR9. *PLoS Pathog* 2017;13, e1006315–e1006315.
- Wang C, Lau CY, Ma F, Zheng C. Genome-wide screen identifies curli amyloid fibril as a bacterial component promoting host neurodegeneration. *Proc Natl Acad Sci U S A* 2021;118:e2106504118.
- Chen SG, Stribinskis V, Rane MJ, et al. Exposure to the functional bacterial amyloid protein curli enhances alpha-synuclein aggregation in aged Fischer 344 rats and *Caenorhabditis elegans*. *Sci Rep* 2016;6:34477.
- Sampson TR, Challis C, Jain N, et al. A gut bacterial amyloid promotes  $\alpha$ -synuclein aggregation and motor impairment in mice. *eLife* 2020;9:e53111.
- Derebe MG, Zlatkov CM, Gattu S, et al. Serum amyloid A is a retinol binding protein that transports retinol during bacterial infection. *eLife* 2014;3:e03206.
- Sack GH Jr. Serum amyloid A - a review. *Mol Med* 2018;24:46.
- Baranova IN, Bocharov AV, Vishnyakova TG, et al. CD36 is a novel serum amyloid A (SAA) receptor mediating SAA binding and SAA-induced signaling in human and rodent cells. *J Biol Chem* 2010;285:8492–8506.
- Deguchi A, Tomita T, Omori T, et al. Serum amyloid A3 binds MD-2 to activate p38 and NF- $\kappa$ B pathways in a MyD88-dependent manner. *J Immunol* 2013;191:1856–1864.
- Yu Y, Liu J, Li S-Q, et al. Serum amyloid a differentially activates microglia and astrocytes via the PI3K pathway. *J Alzheimers Dis* 2014;38:133–144.
- Patel S, Meilandt WJ, Erickson RI, et al. Selective inhibitors of dual leucine zipper kinase (DLK, MAP3K12) with activity in a model of Alzheimer’s disease. *J Med Chem* 2017;60:8083–8102.
- Verschuuren M, Verstraelen P, Garcia G, et al. High-throughput microscopy exposes a pharmacological window in which dual leucine zipper kinase inhibition preserves neuronal network connectivity. *Acta Neuropathol Commun* 2019;7:93.
- Ahmadzai MM, Seguella L, Gulbransen BD. Circuit-specific enteric glia regulate intestinal motor neurocircuits. *Proc Natl Acad Sci U S A* 2021;118:e2025938118.
- Chen CL, Liang TM, Chen HH, et al. Constipation and its associated factors among patients with dementia. *Int J Environ Res Public Health* 2020;17:9006.
- Patke S, Srinivasan S, Maheshwari R, et al. Characterization of the oligomerization and aggregation of human serum amyloid A. *PLoS One* 2013;8:e64974.
- De Buck M, Gouwy M, Wang JM, et al. Structure and expression of different serum amyloid A (SAA) variants and their concentration-dependent functions during host insults. *Curr Med Chem* 2016;23:1725–1755.

25. Man AL, Bertelli E, Rentini S, et al. Age-associated modifications of intestinal permeability and innate immunity in human small intestine. *Clin Sci* 2015;129:515–527.
26. Parikh K, Antanaviciute A, Fawcner-Corbett D, et al. Colonic epithelial cell diversity in health and inflammatory bowel disease. *Nature* 2019;567:49–55.
27. Krueger D, Michel K, Zeller F, et al. Neural influences on human intestinal epithelium in vitro. *J Physiol* 2016; 594:357–372.
28. Wilms E, Troost FJ, Elizalde M, et al. Intestinal barrier function is maintained with aging – a comprehensive study in healthy subjects and irritable bowel syndrome patients. *Sci Rep* 2020;10:475.
29. Tannock LR, De Beer MC, Ji A, et al. Serum amyloid A3 is a high density lipoprotein-associated acute-phase protein. *J Lipid Res* 2018;59:339–347.
30. Lin A, Liu J, Gong P, et al. Serum amyloid A inhibits astrocyte migration via activating p38 MAPK. *J Neuroinflamm* 2020;17:254.
31. Lee JY, Hall JA, Kroehling L, et al. Serum amyloid A proteins induce pathogenic Th17 cells and promote inflammatory disease. *Cell* 2020;180:79–91.e16.
32. Cosolo A, Jaiswal J, Csordás G, et al. JNK-dependent cell cycle stalling in G2 promotes survival and senescence-like phenotypes in tissue stress. *eLife* 2019;8:e41036.
33. Le Pichon CE, Meilandt WJ, Dominguez S, et al. Loss of dual leucine zipper kinase signaling is protective in animal models of neurodegenerative disease. *Sci Transl Med* 2017;9:eaag0394.
34. Mitsuyama K, Suzuki A, Tomiyasu N, et al. Pro-inflammatory signaling by Jun-N-terminal kinase in inflammatory bowel disease. *Int J Mol Med* 2006;17:449–455.
35. Waetzig GH, Seeger D, Rosenstiel P, et al. p38 mitogen-activated protein kinase is activated and linked to TNF- $\alpha$  signaling in inflammatory bowel disease. *J Immunol* 2002;168:5342–5351.
36. Bessho S, Grando KCM, Kyrylchuk K, et al. Systemic exposure to bacterial amyloid curli alters the gut mucosal immune response and the microbiome, exacerbating Salmonella-induced arthritis. *Gut Microbes* 2023;15: 2221813.
37. Miller AL, Pasternak JA, Medeiros NJ, et al. In vivo synthesis of bacterial amyloid curli contributes to joint inflammation during *S. Typhimurium* infection. *PLoS Pathog* 2020;16:e1008591.
38. Nicastro LK, Tursi SA, Le LS, et al. Cytotoxic curli intermediates form during Salmonella biofilm development. *J Bacteriol* 2019;201, e000951-9.
39. Grundmann D, Klotz M, Rabe H, et al. Isolation of high-purity myenteric plexus from adult human and mouse gastrointestinal tract. *Sci Rep* 2015;5:9226.
40. Modolo L, Lerat E. UrQt: an efficient software for the Unsupervised Quality trimming of NGS data. *BMC Bioinformatics* 2015;16:137.
41. Evguenia Kopylova, Laurent Noé, H el ene Touzet. Sort-MeRNA: fast and accurate filtering of ribosomal RNAs in metatranscriptomic data. *Bioinformatics* 2012; 28:3211–3217.
42. Liao Yang, Smyth Gordon K, Shi Wei. The R package Rsubread is easier, faster, cheaper and better for alignment and quantification of RNA sequencing reads. *Nucleic Acids Research* 2019;47:e47.
43. Love MI, Huber W, Anders S. Moderated estimation of fold change and dispersion for RNA-seq data with DESeq2. *Genome Biol* 2014;15:550.
44. Zhou Y, Zhou B, Pache L, et al. Metascape provides a biologist-oriented resource for the analysis of systems-level datasets. *Nat Commun* 2019;10:1523.
45. Zhou Y, Zhou B, Pache L, et al. Metascape provides a biologist-oriented resource for the analysis of systems-level datasets. *Nat Commun* 2019;10:1523.
46. Shannon P, Markiel A, Ozier O, et al. Cytoscape: a software environment for integrated models of biomolecular interaction networks. *Genome Res* 2003;13:2498–2504.
47. Schindelin J, Rueden CT, Hiner MC, et al. The ImageJ ecosystem: an open platform for biomedical image analysis. *Mol Reprod Dev* 2015;82:518–529.
48. De Vos WH, Van Neste L, Dieriks B, et al. High content image cytometry in the context of subnuclear organization. *Cytom A* 2010;77:64–75.

---

Received August 16, 2022. Accepted March 18, 2024.

#### Correspondence

Address correspondence to: Winnok H. De Vos, PhD, Laboratory of Cell Biology and Histology, Universiteitsplein 1, 2610 Wilrijk, Belgium. e-mail: [winnok.devos@uantwerpen.be](mailto:winnok.devos@uantwerpen.be).

#### Acknowledgments

The authors thank Dr Esther Bartholomeus of the Center for Medical Genetics, University of Antwerp, for technical support during RNA sequencing.

#### CRedit Authorship Contributions

Peter Verstraelen (Data curation: Lead; Formal analysis: Lead; Funding acquisition: Supporting; Investigation: Lead; Methodology: Equal; Visualization: Lead; Writing – original draft: Equal; Writing – review & editing: Equal)  
 Samuel Van Remoortel (Investigation: Supporting; Methodology: Equal)  
 Nouchin De Loose (Investigation: Supporting; Methodology: Supporting)  
 Rosanne Verboven (Investigation: Supporting; Methodology: Supporting)  
 Gerardo Garcia-Diaz Barriga (Formal analysis: Supporting)  
 Anne Christmann (Investigation: Supporting; Methodology: Supporting)  
 Manuela Gries (Investigation: Supporting; Methodology: Supporting)  
 Shingo Bessho (Investigation: Supporting)  
 Jing Li (Resources: Supporting)  
 Carmen Guerra (Resources: Supporting)  
 Cagla Tukul (Resources: Supporting)  
 Sales Ibiza Martinez (Methodology: Supporting)  
 Karl-Herbert Schafer (Methodology: Supporting)  
 Jean-Pierre Timmermans (Conceptualization: Equal; Funding acquisition: Lead; Supervision: Equal)  
 Winnok H De Vos (Conceptualization: Equal; Funding acquisition: Lead; Supervision: Equal; Writing – original draft: Equal; Writing – review & editing: Equal)

#### Conflicts of interest

The authors disclose no conflicts.

#### Funding

This work was funded by The Research Foundation Flanders projects G017618N (J.P.T. and W.D.V.), I003420N (W.D.V.), and International Research Infrastructure I000123N (W.D.V.); the University of Antwerp TOP-BOF project 35020 (J.P.T. and W.D.V.) and BOF-KP 39616 (P.V.); and Stichting Alzheimer Onderzoek SAO-FRA 20230041 (W.D.V. and P.V.). Also funded by The Instituto de Salud Carlos III grant PI19/00514, cofunded by European Regional Development Fund “A way of making Europe” and Carmen Delgado/Miguel P erez Mateo Grants third edition “Asociaci n Cancer de P ancreas” & “Asociaci n Espa ola de Pancreatolog a (C.G.); the State Scholarship Foundation of China grant 201609505012 (J.L.); and National Institutes of Health grants AI153325, AI151893, AI148770, and AI171568 (C.T.).

#### Data Availability

All data, images, and image analysis scripts are available upon request. The CellBlocks script for quantification of cell images is available from GitHub (<https://github.com/DeVosLab>).